Structural and optical properties of alloyed quaternary CdSeTeS core and CdSeTeS/ZnS core-shell quantum dots

Oluwasesan Adegoke[a], Tebello Nyokong[b], Patricia B.C. Forbes[a] *

[a]*Department of Chemistry, Faculty of Natural and Agricultural Sciences, University of Pretoria, Lynnwood Road, Pretoria 0002, South Africa*
[b]*Department of Chemistry, Rhodes University, Grahamstown 6140, South Africa*

Abstract

Synthesis of fluorescent alloyed quantum dots (QDs) with unique optical properties suitable for a wide array of chemical, physical and biological applications is of research interest. In this work, highly luminescent and photostable alloyed quaternary CdSeTeS core QDs of two different sizes were fabricated via the organometallic hot-injection synthetic route. Characterization of the nanocrystals were performed using TEM, XRD, UV/vis and fluorescence spectrophotometric techniques. We have demonstrated in this work that the well fabricated alloyed quaternary CdSeTeS core QDs possess unique optical properties that are advantageous over conventional core/shell systems. Formation of the CdSeTeS/ZnS core/shell with the desired optical properties comes with a number of challenges, hence the advantages of the quaternary alloyed core over the core/shell QDs are (i) avoidance of the challenging process of determining the proper shell thickness which can provide the desired optical properties in the core/shell system and (ii) avoidance of the lattice-induced mismatch between the core and the shell material which can either lead to incomplete exciton confinement or dislocation at the core/shell interface.

Keywords: Quantum dots, core/shell, photoluminescence, quantum yield, alloy

*Corresponding author:

Email address: adegoke.sesan@mailbox.co.za (O. Adegoke), t.nyokong@ru.ac.za (T. Nyokong), patricia.forbes@up.ac.za (P.B.C. Forbes)

1. Introduction

The unprecedented research boom that has occurred over the past two decades with respect to the chemistry of semiconductor nanocrystal quantum dots (QDs) stems from their intriguing electronic and optical properties such as their high surface-to-volume-ratio, size-tunable photoluminescence (PL) spectra, narrow emission and broad absorption spectra, bright fluorescence and high resistance to photo-initiated degradation **[1-5].** Due to these unique optical properties, QDs have been exploited significantly in processes that require downshifting of light, especially in scientific and technological applications that rely on achieving unique spectral purity at optimum optical flux. Examples of such applications include: optoelectronic devices **[6]**, molecular biology **[7]**, chemical/biological sensing **[8,9]**, bioimaging **[10],** photochemistry **[11],** etc.

QD features such as their strong coulombic interactions and the excitonic confinement phenomenon exhibited, for example, by non-alloyed binary cores composed of group II-VI semiconductors of ZnTe, ZnSe, CdSe, CdTe and CdS are now well documented in the literature **[12-15]**. Among these examples, CdTe and CdSe QDs are the most popular and widely studied. However, certain limitations with reference to their optical properties have inspired researchers to modify their surfaces. The main limitations with binary Cd-based cores are their low PL quantum yields and reduced photostability. This is due to surface dangling bonds or trap

states which act as rapid radiationless recombination channels for photo-initiated charge carriers **[16].** Synthesizing QDs that ultimately solve the problems of low PL QY and photostability is therefore of research interest. Hence, modification strategies such as the fabrication of alloyed QDs and passivation of cores with shell layers have been employed to improve the qualities of binary CdTe and CdSe-based QDs.

Alloyed QDs have attracted research attention in recent years due to the possibility of fine-tuning their composition and size-dependent electronic and optical properties **[17]**. For example, CdSeTe QDs, the first cadmium-based alloyed ternary nanocrystals, were synthesized by Nie at al., in 2003 **[18]** and since then several other types of ternary cores composed of CdZnTe **[19]**, CdZnSe **[20]** and CdZnS **[21]** have been reported in literature with superior optical features than those of conventional binary CdTe and CdSe QDs. Additionally, scientific progress has also been made in the synthesis of quaternary alloyed cores composed of ZnCdSSe **[22],** CdZnTeSe **[23]**, and CdSeTeS **[24].** To the best of our knowledge, the synthesis of alloyed quaternary CdSeTeS core QDs, which is of interest in this work, have only been reported once in literature and they were synthesized via a microwave assisted aqueous method **[24].**

In this work, we report for the first time on the organometallic hot-injection synthesis of alloyed quaternary CdSeTeS core and CdSeTeS/ZnS core/shell QDs exhibiting high PL quantum yield (QY) in organic solvent. Water-soluble nanocrystals were obtained via a ligand exchange reaction with L-cysteine as a thiol capping agent. Our primary objective in this work is to demonstrate that alloyed quaternary core QDs can serve as an alternative to providing improved optical properties without the need for further shell coating. An additional motivation for

coating the quaternary alloyed core QDs with a wider band gap ZnS shell is to be able to draw a meaningful scientific conclusion regarding the optical properties of the quaternary core and quaternary core/shell QDs. Furthermore, we believe this new generation of QDs will result in enhanced performance in applications ranging from light-emitting devices to fluorescence sensing and biological multiplexed tracking and labelling.

2. Experimental Section

2.1. Materials

Trioctylphosphine oxide (TOPO), cadmium oxide, sulphur, 1-octadecene (ODE), tellurium powder, L-cysteine, and oleic acid (OA) were purchased from Sigma Aldrich. Methanol, chloroform, zinc powder, acetone, selenium powder and potassium hydroxide were purchased from Merck. Hydrophobic QDs were prepared in chloroform while hydrophilic QDs were prepared with ultra pure water obtained from a Milli-Q Water System.

2.2. Characterization

UV-vis absorption spectra were recorded on a Cary Eclipse (Varian) spectrophotometer. Fluorescence emission spectra were recorded on a Horiba Jobin Yvon Fluoromax-4 spectrofluorometer. Determination of the PL quantum yield (Φ_F) of the QDs was achieved by comparing the integrated fluorescence intensities of the QDs (F) in Millipore water (for hydrophilic QDs) or chloroform (for hydrophobic QDs) to that of Rhodamine 6G (F_{Std} ; $\Phi_{F(Std)}$ = 95% **[25]**) in ethanol whilst taking into

consideration the refractive indices (n) of the solvents and absorbance of each QDs (A) and Rhodamine 6G (A_{Std}) at the excitation wavelength.

$$\Phi_F = \Phi_{F(Std)} \frac{F \,.\, A_{Std} \,.\, n^2}{F_{Std} \,.\, A \,.\, n_{Std}^2} \qquad [\mathbf{19}]$$

Powder X-ray powder diffraction (XRD) patterns were analyzed using a PANalytical X'Pert Pro powder diffractometer in θ–θ configuration with an X'Celerator detector, variable divergence and receiving slits with Fe filtered Co-Kα radiation (λ=1.789Å). Transmission electron microscopy (TEM) images were obtained using a JEOL JEM 2100F operated at 200 kV. Fluorescence lifetime measurements were carried out using a time correlated single photon counting (TCSPC) setup (FluoTime 300, Picoquant GmbH). The excitation source was a diode laser (LDH-P-670 and LDH-P-481 with PDL 800-B, Picoquant GmbH, 20 MHz repetition rate, 44 ps pulse width). To obtain good statistics, the ratio of stop to start pulses was kept low (below 0.05). Data analysis was done using the program Fluofit (Picoquant GmbH). Estimation of the decay error times was carried out using the support plane approach.

2.3. Synthesis of CdSeTeS and CdSeTeS/ZnS QDs

2.3.1. Preparation of the precursors

In order to prepare the Se and Te precursors, 1.93 g of TOPO was dissolved in 25 mL of ODE and heated to 80 ^{o}C to obtain a clear solution. Then 0.3 g of Se and 0.48 g of Te were added into separate solutions of TOPO and stirred continuously to generate the TOPSe and TOPTe precursors. Zinc and sulphur precursors were prepared by dissolving 0.16 g of sulphur and 0.407 g of zinc powder in separate solutions of a mixture of 20 mL OA and 30 mL ODE.

2.3.2. Fabrication of the QDs

Quaternary alloyed CdSeTeS core and CdSeTeS/ZnS core/shell QDs were synthesized via a one-step organometallic hot-injection approach, using a modification of the one-pot synthetic method for core/shell QDs **[26].** In a three-necked flask fitted with a refluxing condenser, septum and thermometer, 1.3 g of CdO was added into a mixture of 30 mL OA and 50 mL ODE to give a brownish mixture which was heated up under vigorous stirring. When the temperature reached ~280 ^{o}C, the solution turned clear and the TOPSe precursor (15 mL) was added into the Cd-OA mixture to allow for nucleation and growth of CdSe QDs. After ~2 min of forming the CdSe QDs, 5 mL of the TOPTe precursor was added to initiate the nucleation and growth of the alloyed CdSeTe QDs. The reaction was allowed to proceed for 15 min whereafter the sulphur precursor was added to initiate the formation of quaternary alloyed CdSeTeS QDs. Two sizes of the quaternary CdSeTeS QDs (denoted as CdSeTeS1 and CdSeTeS2) were harvested at emission wavelengths > 600 nm.

To passivate the alloyed core surface, we adopted the selective ion adsorption and reaction (SILAR) approach **[27]** to epitaxially overgrow the ZnS shell layer. At different time intervals, separate solutions of zinc and sulphur precursors were added into the CdSeTeS solution at a reduced temperature of 240 ^{o}C. Two portions of the CdSeTeS/ZnS QDs with different shell thickness were harvested at reaction times of 75 and 105 min (denoted as CdSeTeS/ZnS1 and CdSeTeS/ZnS2 with 1 and 2 ML of ZnS shell). The QDs were purified using methanol and centrifuged

repeatedly with a solution of acetone and an acetone:chloroform (1:1) mixture was further employed to completely remove unreacted precursors.

2.3.3. Water-solubilization of the QDs

Water solubilisation of the QDs was achieved via ligand exchange reaction of the hydrophobic capping (OA and TOPO) with the hydrophilic thiol L-cysteine (L-cys) ligand. Typically, L-cysteine-KOH methanolic stock solution was prepared by adding 2 g of L-cysteine to 3.0 g of KOH in 40 mL methanol with dissolution assisted by ultrasonication. The purified OA-TOPO-capped CdSeTeS and CdSeTeS/ZnS QDs were re-dispersed in chloroform and the L-cysteine-KOH methanolic solution was subsequently added followed by the addition of Millipore water separately to each QD solution. The solutions were stirred for 1 hr for effective separation of the organic phase from the aqueous phase. The water-soluble QDs thus obtained were purified repeatedly via centrifugation with acetone followed by a water:chloroform:acetone (1:1:2) mixture to completely remove all unreacted organic substituents. The purified aqueous dispersible QDs were dried in a fume hood.

3. Results and discussion

3.1. Structural properties

Powder XRD patterns for the hydrophobic (Fig. 1) and L-cys-capped (see Fig. S-1 in supplementary information) CdSeTeS core and CdSeTeS/ZnS core/shell QDs depicts a consistent single crystalline domain feature. Both the core and core/shell QDs exhibit a zinc-blend crystal structure with planes at {111}, {220} and {311}

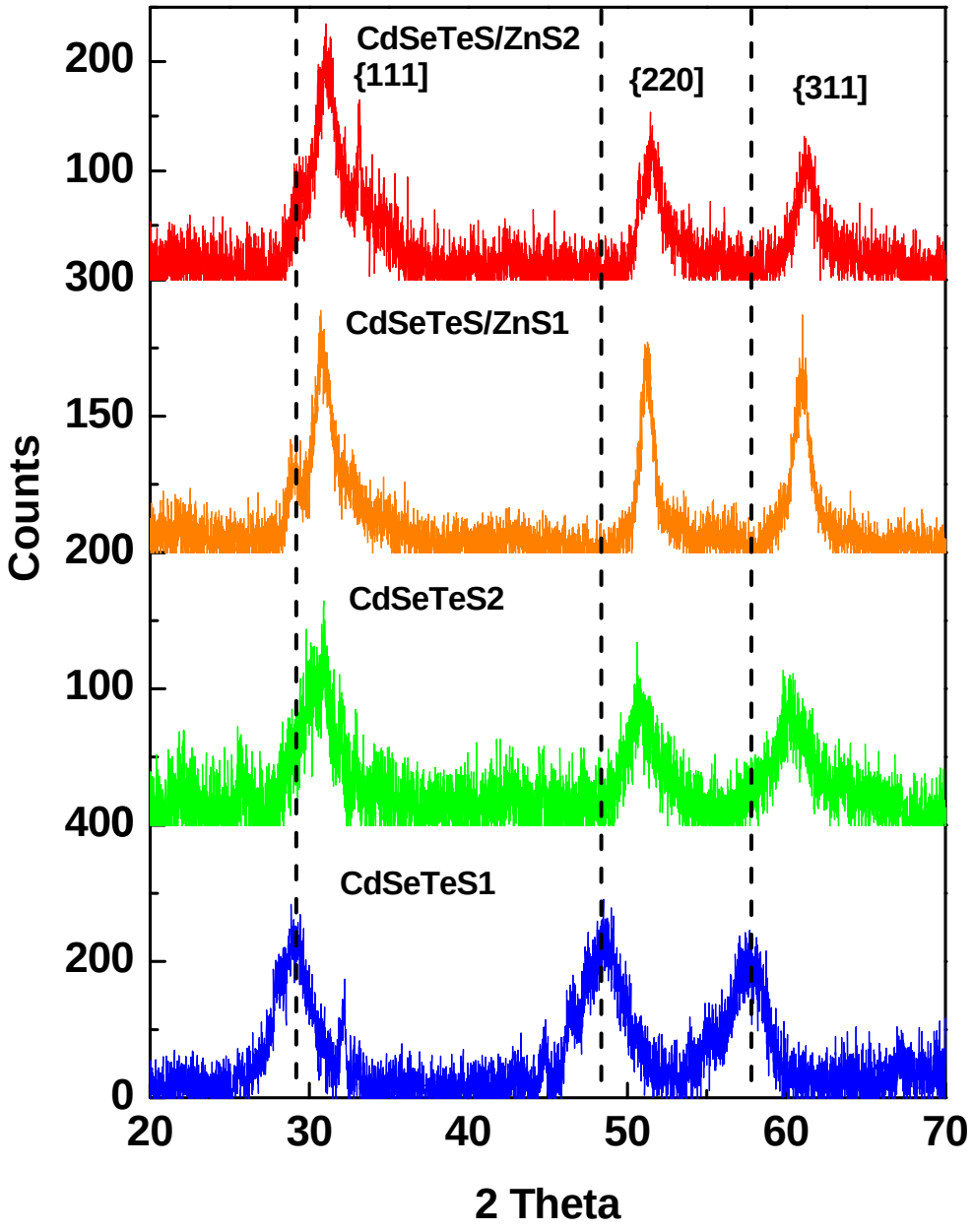

Fig. 1. XRD patterns for the hydrophobic CdSeTeS1, CdSeTeS2, CdSeTeS/ZnS1 and CdSeTeS/ZnS2 QDs.

respectively. For the hydrophobic core QDs, a shift to higher Bragg angle was observed with increase in size (Fig. 1). Upon 1 ML of ZnS shell deposition, further shift of the diffraction peaks to higher Bragg angle was observed and when an additional 2 ML of ZnS shell was deposited, the diffraction peaks shifted slightly to higher Bragg angle. The existence of the peak shift confirms both the size increase and shell formation. Furthermore, the unchanged phase of the zinc-blende crystal structure of the core/shell QDs confirms an epitaxial shell growth **[28]**. It is important to note that the diffraction peaks also became narrower as the crystalline size domain increased.

XRD patterns for the water-soluble L-cys-capped QDs shown in Fig. S-1 are less shifted to higher Bragg angle when compared to the hydrophobic QDs (Fig. 1). Although, there were similarities in the diffraction patterns for both the hydrophobic and water-soluble QDs, the replacement of the hydrophobic capping with L-cys thiol ligand played a critical role in the surface properties of the water-soluble QDs and thus the shift to higher Bragg angle upon size increase and shell deposition is small relative to the hydrophobic nanocrystals. Generally, we believe the original crystal structure of the core QDs which was maintained in the core/shell domain is due to the epitaxial shell growth **[28].**

TEM analysis was carried out to enable qualitative probing of the internal morphology and average particle size distribution of the QDs. We imaged both the hydrophobic and L-cys-capped QDs respectively. TEM images for the hydrophobic QDs are shown in Fig. 2A- 2D while the corresponding L-cys-capped QDs are shown in Fig. S-2 in supplementary information. The shape of the particles for the core QDs

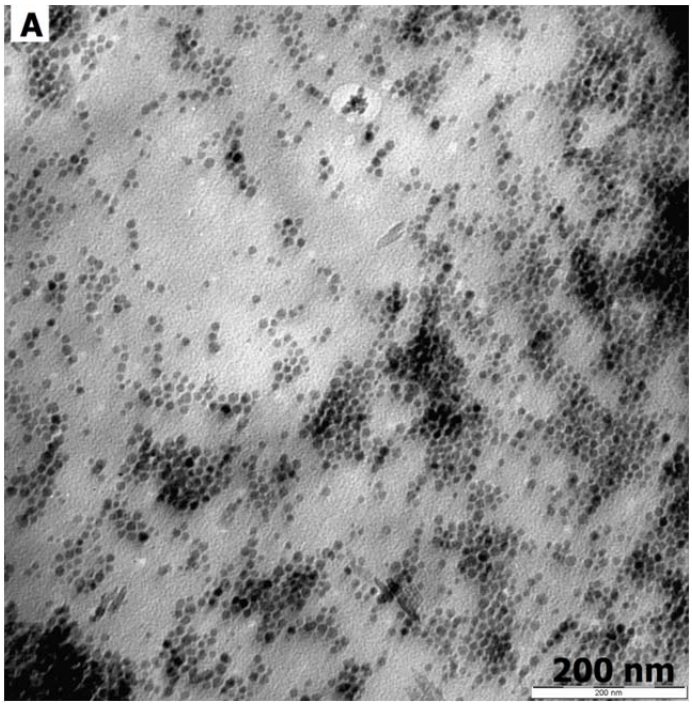
A
200 nm

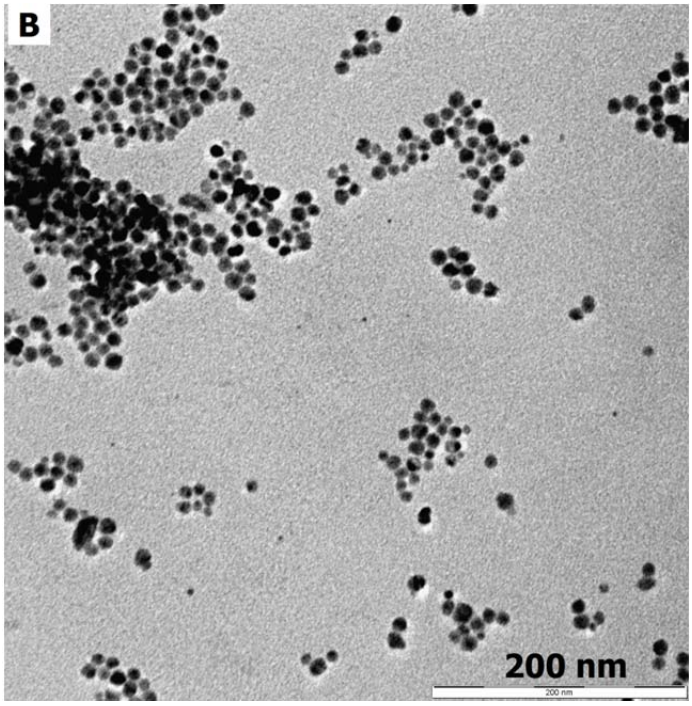
B
200 nm

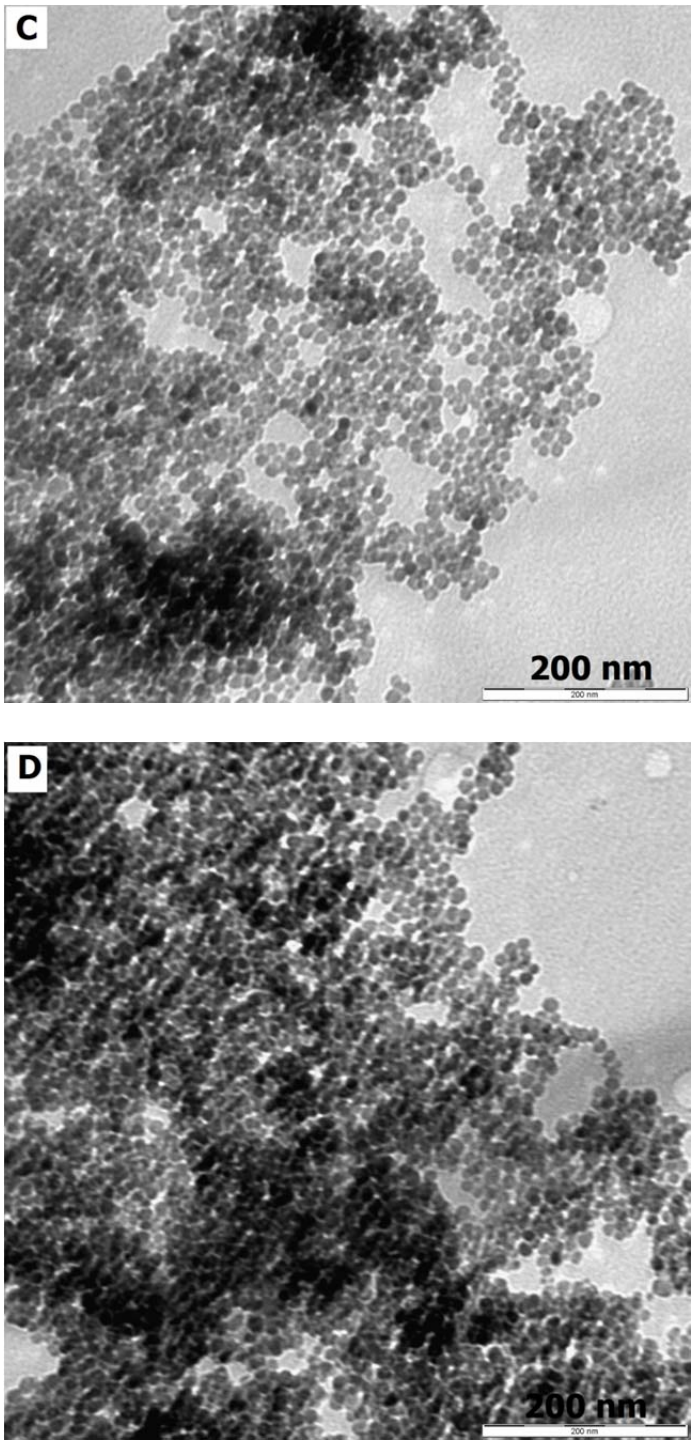

Fig. 2. TEM images of hydrophobic (A) CdSeTeS1, (B) CdSeTeS2, (C) CdSeTeS/ZnS1 and (D) CdSeTeS/ZnS2 QDs.

shows they are spherical while the particle size distribution was monodispersed. As the core/shell QDs were formed, less uniformity and homogeneity was observed. Interestingly, we observed with reference to the shape and particle size distribution of the QDs, that there were similarities in the TEM images for the hydrophobic and L-cys-capped core and core/shell QDs. CdSeTeS1 and CdSeTeS2 QDs (referring to both hydrophobic and water-soluble forms) remained monodispersed but upon shell coverage, the monodispersity decreased as the shell thickness increased. Histograms depicting the average size distribution of the QDs are shown in Fig. 3. Since L-cys-capped QDs were obtained via ligand exchange of the organic capping of the hydrophobic QDs, it is reasonable to assume the same core and core/shell size. Hence, the hydrophobic QDs were used as a representative sample to determine the average size distribution of the QDs. The average sizes of CdSeTeS1 and CdSeTeS2 QDs were measured to be 4.0 and 4.7 nm while CdSeTeS/ZnS1 and CdSeTeS/ZnS2 containing 1 and 2 ML of ZnS shell were found to be 5.2 and 5.3 nm respectively. Using TEM, we have indirectly measured the ZnS shell thickness by subtracting the average particle size of CdSeTeS2 from CdSeTeS/ZnS1 and CdSeTeS/ZnS2 **[29].** The measured ZnS thickness for CdSeTeS/ZnS1 QDs was 0.5 nm while that of CdSeTeS/ZnS2 QDs was 0.6 nm. However, we have to take into consideration that TEM generally provides insufficient contrast at the edges of the nanoparticle, hence the calculated thickness of the ZnS layer could present an uncertainty of ~10-15% **[29]**.

3.2. Optical properties

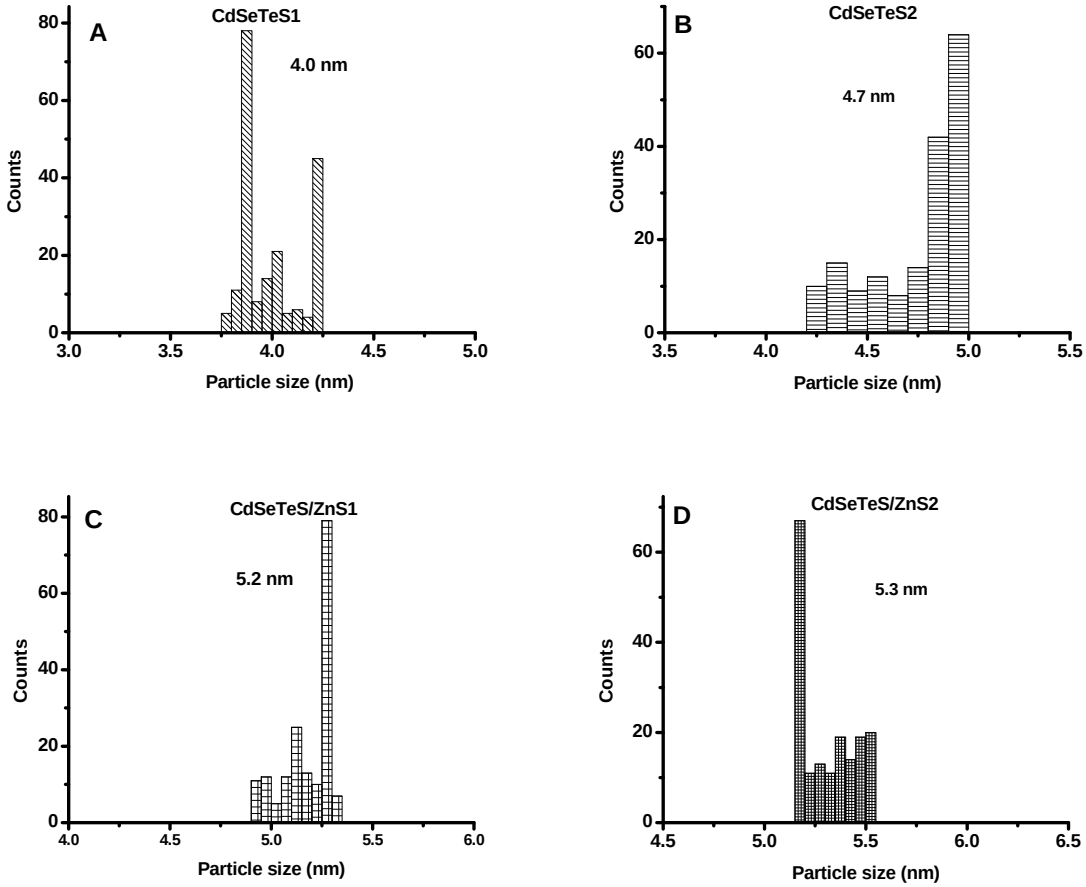

Fig. 3. Histograms depicting the particle size distribution of the hydrophobic QDs, which are regarded as being representative with respect to particle size distribution of both hydrophobic and hydrophilic QDs. (A) CdSeTeS1, (B) CdSeTeS2, (C) CdSeTeS/ZnS1 and (D) CdSeTeS/ZnS2 QDs.

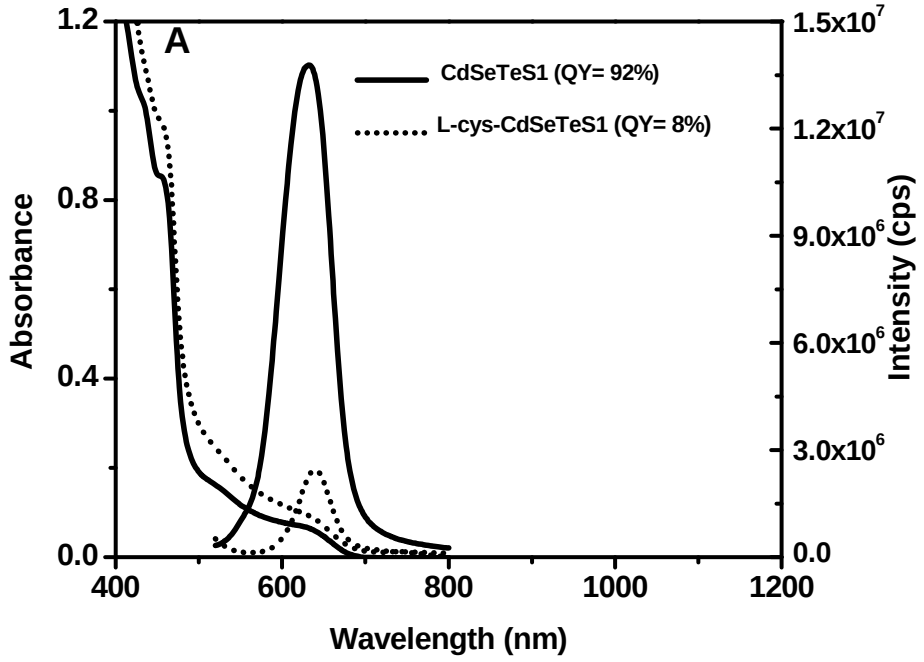
A
CdSeTeS1 (QY= 92%)
L-cys-CdSeTeS1 (QY= 8%)
Absorbance
Intensity (cps)
Wavelength (nm)
1.2
0.8
0.4
0.0
1.5x10^7
1.2x10^7
9.0x10^6
6.0x10^6
3.0x10^6
0.0
400
600
800
1000
1200

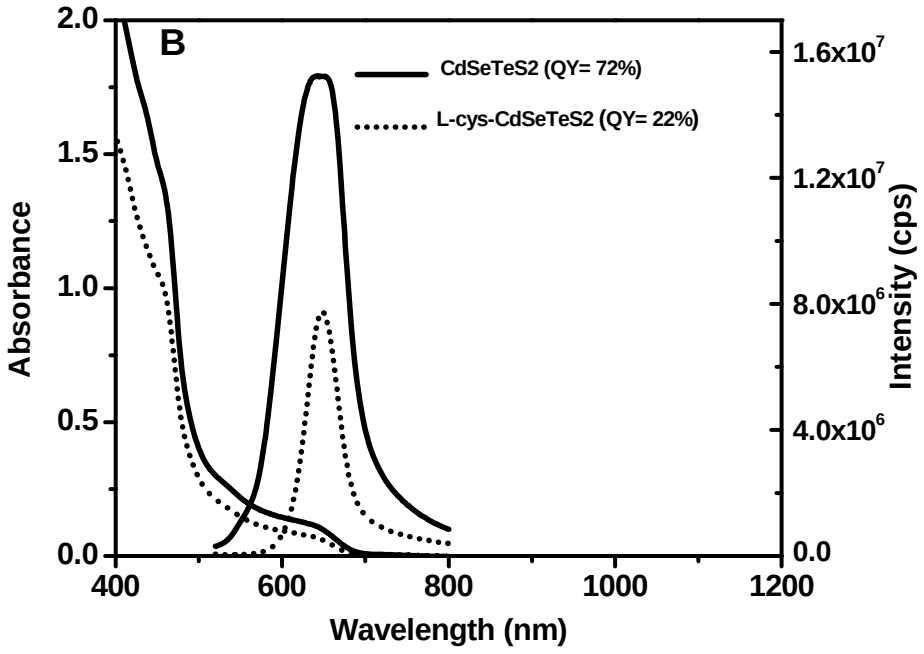
B
CdSeTeS2 (QY= 72%)
L-cys-CdSeTeS2 (QY= 22%)
Absorbance
Intensity (cps)
Wavelength (nm)
2.0
1.5
1.0
0.5
0.0
1.6x10^7
1.2x10^7
8.0x10^6
4.0x10^6
0.0
400
600
800
1000
1200

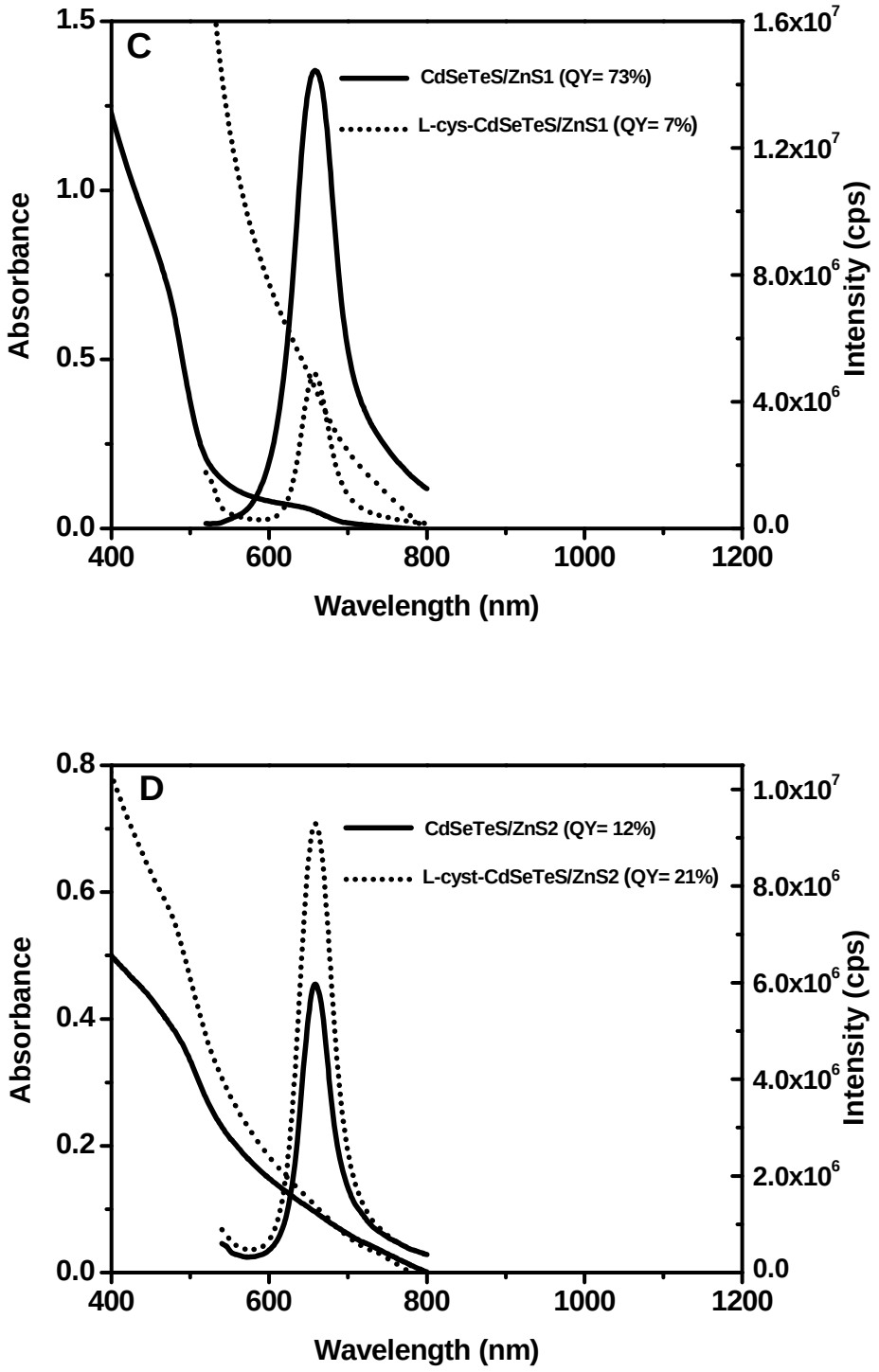

Fig. 4. Absorption, PL emission spectra and QY values of hydrophobic and L-cysteine-capped (A) CdSeTeS1, (B) CdSeTeS2, (C) CdSeTeS/ZnS1 and (D) CdSeTeS/ZnS2 QDs. λ_{exc} = 500 nm.

Fig. 4A–4D shows the absorption spectra before (solid lines) and after (dotted line) conversion of the hydrophobic QDs to water-soluble nanocrystals. For the core QDs, an excitonic absorption peak was clearly observed for both the hydrophobic and water-soluble nanocrystals and this was accompanied by a small shift to the red region (lower energies) for CdSeTeS2 QDs relative to CdSeTeS1 QDs. There were also similarities in the absorption spectra of the core QDs even after conversion to the water phase. Upon shell coverage, we observed that the excitonic absorption peak was noticeable for the hydrophobic CdSeTeS/ZnS1 QDs but broadened upon conversion to the water phase. On the other hand, the broadening of the absorption spectra was pronounced for both hydrophobic and water-soluble CdSeTeS/ZnS2 QDs. The broadening suggests that as the core/shell QDs grew with time, the size distribution of the dots widened, leading to a broader absorption range. TEM images and related histograms of the core/shell QDs shown in Fig. 2 and Fig. 3 verify their high dispersity and also assist in understanding the absorption spectral broadening behaviour. The corresponding room-temperature PL spectra of the CdSeTeS cores measured before (solid line) and after (dotted line) conversion to the water-soluble phase are shown in Fig. 4A-4B. Table 1 provides a summary of the photophysical properties of these nanocrystals. Hydrophobic CdSeTeS1 QDs with an emission wavelength of 632 nm produced a high PL QY value of 92% but this reduced dramatically to 8% upon conversion to the water-soluble phase. This represents a 91% drop in PL intensity upon ligand exchange with L-cys. We also noticed a red-shift of 7 nm for the L-cys-capped CdSeTeS1 QDs (639 nm) relative to its hydrophobic form. The red-shift provides direct evidence of the presence of L-cys

capping on the surface of the QDs and its influence on the PL emission specta of the QDs. A 10 nm red-shift in the PL emission wavelength of hydrophobic CdSeTeS2 QDs (642 nm) relative to the CdSeTeS1 QDs was observed and thus provides direct evidence that the alloyed quaternary QDs grew with reaction time. The size-dependent PL emission peak shift can generally be attributed to the quantum size behaviour of semiconductor nanoparticles of size <10 nm **[30]**. Similarly, the hydrophobic CdSeTeS2 QDs red-shifted by 7 nm upon conversion to the water-soluble phase (649 nm). PL QY measurements of hydrophobic CdSeTeS2 QDs dropped to a value of 72 % probably due to quenching by prolonged reaction time. However, from a scientific point of view, this value is still relatively high and provides evidence that CdSeTeS2 QDs are still of high quality. Upon conversion to the water-soluble phase, a 69% loss in PL emission was observed and the QY value of L-cys-capped CdSeTeS2 QDs dropped to 22%. The ensemble PL emission full width at half maximum (FWHM) values for hydrophobic CdSeTeS1 and CdSeTeS2 QDs were 70 nm and 84 nm respectively, but these values decreased significantly to 48 nm and 46 nm upon conversion to the water-soluble phase (Table 1). This significant reduction may be due to differing uniformity influenced by the presence of surface bound L-cys ligand on the shape and size distribution of the nanocrystals. Generally speaking, the photophysical data for quaternary CdSeTeS core QDs produced in this work, suggests that the optical properties of individual alloyed QDs depends on their size as well as the presence of surface attached ligand.

In order to obtain a clear understanding of the effects of ZnS passivation on the photophysical properties of alloyed quaternary CdSeTeS QDs, we modulated the

shell thickness by depositing 1 and 2 ML of ZnS shell layer. An attempt to deposit more than 2 ML of ZnS shell was not successful in this work. Fig. 4C-4D shows the progression of the PL emission spectra for the CdSeTeS/ZnS core/shell QDs before (solid line) and after (dotted line) conversion to the water-soluble phase. The photophysical parameters of the core/shell QDs are also listed in Table 1. Upon deposition of 1 ML of ZnS shell, the PL emission wavelength of CdSeTeS/ZnS1 QDs (658 nm) red-shifted by 16 nm and this was reflected by a slight increase in the QY value of up to 73%. In comparison to the 16 nm red-shift in PL emission observed for CdSeTeS/ZnS1 relative to CdSeTeS2, the water-soluble L-cys-CdSeTeS/ZnS1 (657 nm) exhibited a slightly reduced emission red shift of 8 nm relative to L-cys-CdSeTeS2. The observed red-shift could be due to strong leakage of the exciton (electron and hole) into the ZnS matrix **[31]**. Also, a dramatic decline in the PL QY value to 7% was observed and this corresponded to a 90% loss in PL emission upon conversion to the water-soluble phase.

In contrast to the slightly improved QY value for CdSeTeS/ZnS1 QDs, the QY value for CdSeTeS/ZnS2 QDs dropped remarkably to 12%. However, the PL emission wavelength was the same for both sets of QDs. The conversion of the hydrophobic CdSeTeS/ZnS2 QDs to the water-soluble phase (L-cys-CdSeTeS/ZnS2), resulted in an appreciable increase in the PL QY to 21% and this is directly evident from the increase in the PL intensity as shown in Fig. 4D. From a scientific point of view, this phenomenon is intriguing because conversion of the hydrophobic QDs to water-soluble forms generally results in PL loss **[32,33]**.

Table 1. Photophysical parameters for hydrophobic and L-cys-capped CdSeTeS core and CdSeTeS/ZnS core/shell QDs.

Nanocrystals	**PL, λ_{emi} (nm)**	**PL QY (%)**	**FWHM**	**Size (nm)**	**Shell thickness (nm)**
CdSeTeS1	632	92	70	4.0[a]	-
CdSeTeS2	642	72	84	4.7[a]	-
CdSeTeS/ZnS1	658	73	60	5.2[a]	0.5
CdSeTeS/ZnS2	658	12	46	5.3[a]	0.6
L-cys-CdSeTeS1	639	8	48	4.0	-
L-cys-CdSeTeS2	649	22	46	4.7	-
L-cys-CdSeTeS/ZnS1	657	7	39	5.2	0.5

L-cys-CdSeTeS/ZnS2	659	21	48	5.3	0.6

[a] Representative with respect to particle size distribution for both hydrophobic and hydrophilic QDs.

Table 2. Time-resolved PL values for CdSeTeS and CdSeTeS/ZnS QDs

QDs	**τ_1 (ns)[a]**	**τ_2 (ns)[a]**	**τ_3 (ns)[a]**	**Mean lifetime (ns)**
CdSeTeS1	24.1(0.09)	4.3(0.29)	0.8(0.62)	9.7
CdSeTeS2	37.4(0.31)	7.9(0.54)	1.0(0.15)	15.4
CdSeTeS/ZnS1	36.0(0.70)	5.5(0.23)	1.0(0.07)	14.2
CdSeTeS/ZnS2	53.6(0.26)	10.7(0.57)	1.6(0.17)	22.0

[a]Relative abundance in brackets

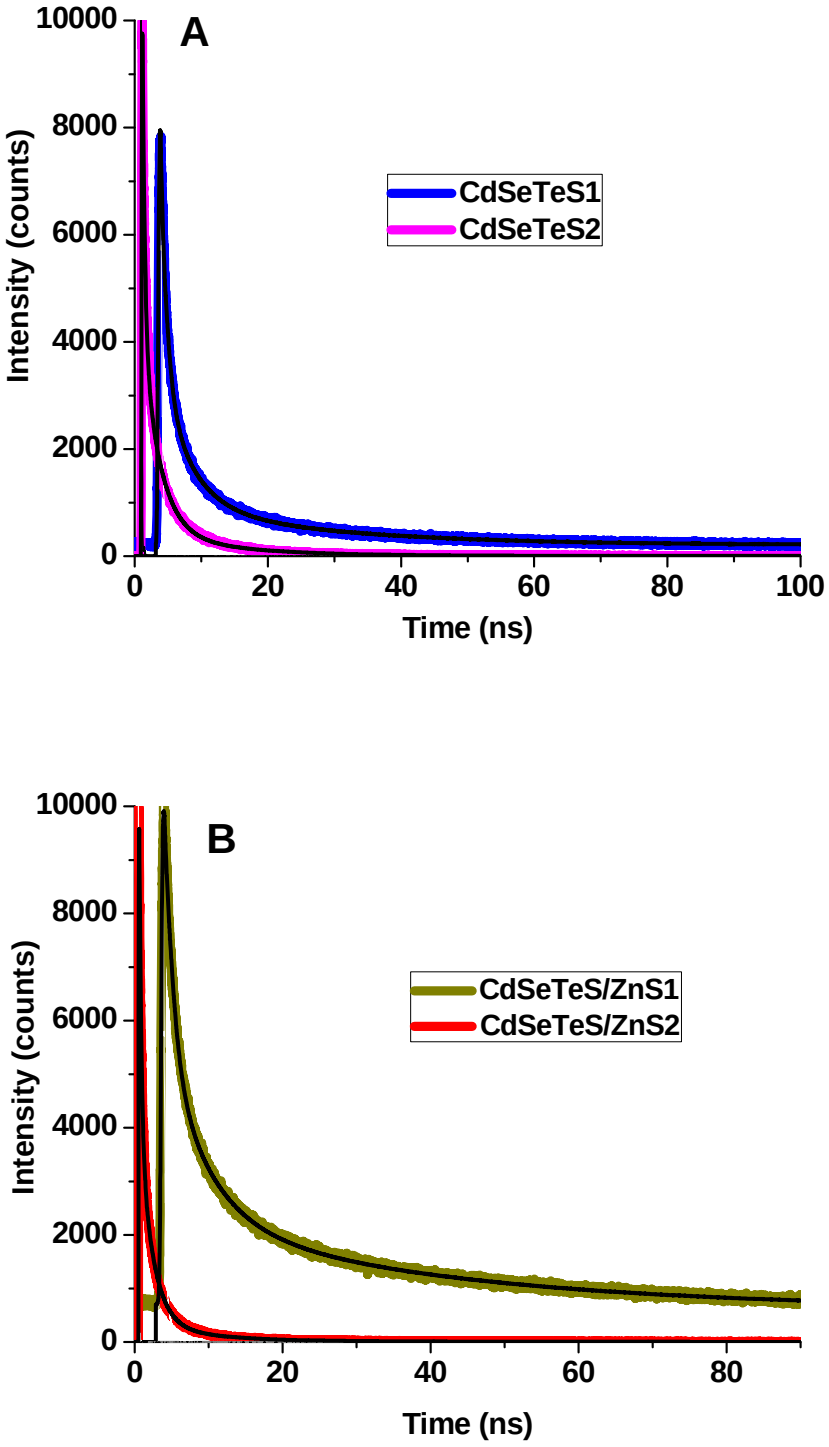

Fig. 5. Time-resolved PL decay curves for (A) CdSeTeS core and (B) CdSeTeS/ZnS core/shell QDs.

In order to understand more clearly the optical changes in the core and core/shell QDs, we believe there should be an intrinsic connection between the PL lifetimes and QY values of the QDs. Hence, we successfully simulated the PL lifetime values of the QDs by fitting each of the core and core/shell QDs to a tri-exponential decay. The hydrophobic QDs have been used as a reference for this study. Fig. 5A and 5B show the PL decay curves of the core and core/shell QDs whilst Table 2 lists the PL lifetime parameters. Comparing the average of each of the τ_1 (longer lifetime), τ_2 (intermediate lifetime) and τ_3 (shortest lifetime) for the core and core/shell QDs, we observed that CdSeTeS1 QDs with a QY value of 92% decayed faster (9.7 ns) than the rest of the QDs (Table 2). Hence, we can use this basis to understand the surface chemistry and internal structure of the remaining QDs. The drop in the QY for CdSeTeS2 (QY = 72%) resulted in a slower decay (15.4 ns) while CdSeTeS/ZnS1 (QY = 73%) produced a slightly faster decay (14.2 ns). CdSeTeS/ZnS2 QDs (QY =12%) on the other hand, exhibited the slowest decay (22.0 ns). Hence, our data provides concrete evidence of the complimentary relationship between the PL QY and lifetime data trends.

We can tentatively draw the conclusion that some level of non-radiative exciton recombination was created in CdSeTeS2 QDs which was then stabilized or slightly minimized upon passivation with 1 ML of ZnS shell. However, the significant drop in PL QY for CdSeTeS/ZnS2 QDs and the fact that it exhibited the slowest decay provides evidence that surface trap formation played a significant influence in its optical properties. However, either of two trap state types are possible as proposed by Jones et al. **[34].** The trap state could be nearer to the alloyed CdSeTeS core at the

core/shell interface or localized within the outer layer of the ZnS surface **[34]**. The former could be referred to as an "interface trap" while the later could be referred to as a "shell trap" **[35].**

3.3. Stability of the QDs

The PL stability of QDs is an important factor required for applications involving continuous output of photons, hence we have investigated the PL stability of both the hydrophobic and water-soluble nanocrystals. The QDs were each dissolved in separate solutions of chloroform (hydrophobic QDs) or Millipore water (aqueous QDs) for 21 days and exposed to ambient light. If the QDs are unstable, precipitation will occur from solution and this will be accompanied by quenching of their PL emission spectra. Fig. 6 and Fig. S-3 shows the changes in the PL intensities of the QDs measured before and after 21 days of exposure to ambient light. Both the hydrophobic and water-soluble core and core/shell QDs displayed excellent stability as evidenced by the lack of PL quenching in their emission intensities and retained emission line width. Most noticeable was the PL enhancement observed after 21 days of measurements for some of the QDs. This practically demonstrates the potential of these nanocrystals for use in a variety of chemical, physical and biological applications.

3.4. General discussion

We attribute the growth of the ZnS shell on the CdSeTeS2 seed nanoparticles by either of three ways: highly disordered, incoherent epitaxial (with strain or

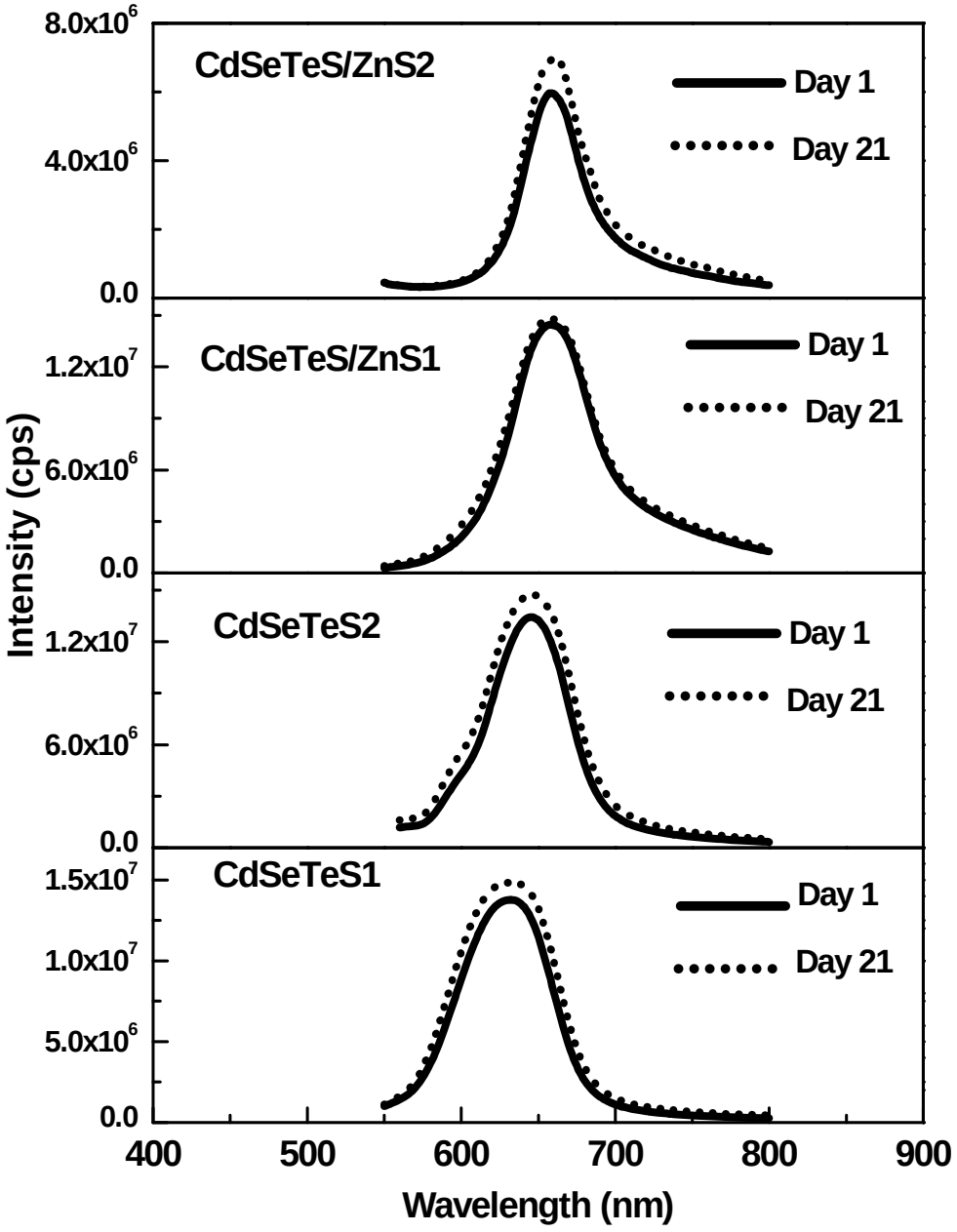

Fig. 6. PL stability of the hydrophobic QDs measured before (solid line) and after 21 days (dotted line) of exposure to ambient light.

dislocation) or coherent epitaxial with high strain or distortion. Since the XRD pattern of the core/shell QDs originated from a crystalline structure, we can directly rule out the possibility of highly disordered shell coverage **[29].** Further elucidation of the other two possibilities is extremely difficult because data obtained from TEM does not provide any direct picture of a lattice plane extension with an interface which practically should be consistent with a coherent epitaxial type of growth mechanism. However, we assume that as the thickness of the shell increased, the formation of low-angle grain boundaries and dislocations could have induced the growth of the ZnS2 shell to occur incoherently. We speculate that this process led to interfacial defect states due to the large lattice mismatch between CdSeTeS and ZnS and hence the QY value of CdSeTeS/ZnS2 QDs declined significantly. To supplement our observation, an attempt to overcoat an additional 3 ML of ZnS shell led to instability of the nanocrystals which may imply that attempts to further increase the shell thickness generated higher misfit dislocation.

While it is an established phenomenon in the chemistry of semiconductor QD nanocrystals to passivate the surface of conventional binary cores against surface defects using shell layers with the prospect of obtaining improved optical properties suitable for a wide array of applications, we have demonstrated in this work that a well fabricated quaternary alloyed core system can serve as an alternative to conventional core/shell systems without employing the challenging process of shell overgrowth. From our data, we have shown that developing highly efficient core/shell systems comes with a number of challenges. Such challenges includes (i) finding a suitable shell thickness that can produce the required optical properties;

and (ii) the large lattice mismatch between the core and shell materials can either induce incomplete exciton confinement or lead to dislocations at the core/shell interface and hence produce unattractive optical properties. Therefore, the prospect of using quaternary alloyed QD cores will eliminate these challenges. However, the two main technical problems which we encountered in the process of fabricating our quaternary alloyed core system were: (i) finding a proper mechanistic mole ratio between the precursor materials. This is of practical importance as it determines the overall quality of the nanocrystal product; (ii) the synthesis of the quaternary alloyed core generated a large quantity of impurities hence making the purification step extremely labour intensive. In order to solve the first problem, a clear understanding of the effects of each precursor material when combined with one another is important. To solve the second problem, the purification steps outlined below were employed depending on the type of QDs: (a) centrifuge in acetone repeatedly and decant supernatant → purification step 1 (b) re-disperse in chloroform (for water-soluble nanocrystals), centrifuge repeatedly and decant supernatant → purification step 2 (c) re-disperse in chloroform:acetone (1:1) for hydrophobic QDs or H_2O:chloroform:acetone (1:1:2) (for water-soluble nanocrystals), centrifuge repeatedly and decant supernatant → purification step 3 (d) re-disperse in chloroform or acetone (for water-soluble nanocrystals), centrifuge repeatedly and decant supernatant → purification step 4.

Finally, as a rare phenomenon, it is difficult to conclude that L-cys effectively passivated the surface of CdSeTeS/ZnS2 against PL loss during the ligand exchange process. The reason for this is that since L-cys was not directly involved in the hot-

injection synthetic process, it is almost inappropriate to attribute the phenomenon of surface passivation as the sole reason for the QY increase. However, we can tentatively conclude that a strong affinity between the surface CdSeTeS/ZnS2 QDs and L-cys capping may have assisted with the ligand exchange process.

4. Conclusions

In summary, the synthesis and characterization of alloyed quaternary CdSeTeS core and CdSeTeS/ZnS core/shell QDs exhibiting high PL QY in organic solvent have been successfully carried out. A decline in the QY values upon conversion of the hydrophobic QDs to water-soluble states was observed with the exception of L-cys-capped-CdSeTeS/ZnS2 QDs which displayed an appreciable increase in the QY value. Complimentary XRD, TEM and PL data provided direct evidence of an epitaxial ZnS shell overgrowth which was accompanied with strain or dislocation at higher shell thickness. In general, our data suggests that the unique optical properties of the alloyed quaternary core QDs can serve as a useful platform in a wide array of applications over conventional core/shell systems.

Acknowledgements

A postdoctoral fellowship offered by the University of Pretoria is gratefully appreciated by O. Adegoke. This work is based on research supported in part by the National Research Foundation of South Africa, Grant Numbers: 92584, 90720 and 93394 (P. Forbes). Wirsam Scientific, South Africa is thanked for their support of this research. We thank the Electron Microscopy Unit, University of Pretoria (UP), for

assistance with the TEM measurements and Wiebke Grote of UP for the XRD measurements.

References

[1] X. Wu, H. Liu, J. Liu, K. N. Haley, J. A. Treadway, J. P. Larson, N. Ge, F. Peale, M. P. Bruchez, Nat. Biotechnol. 21 (2003) 41-46.

[2] A. P. Alivisatos, Science 271 (1996) 933-937.

[3] K. Grieve, P. Mulvaney, F. Grieser, Curr. Opin. Colloid Interface Sci. 5 (2000) 168-172.

[4] P. Alivisatos, Nat. Biotechnol. 22 (2004) 47-52.

[5] M. Nirmal, L. Brus, Acc. Chem. Res. 32 (1999) 407-414.

[6] V. Wood, M.J. Panzer, J. Chen, M.S. Bradley, J.E. Halpert, M.C. Bawendi, V. Bulović, Adv. Mater. 21 (2009) 2151-2155.

[7] V. Biju, A. Anas, H. Akita, E.S. Shibu, T. Itoh, H. Harashima, M. Ishikawa, ACS Nano 6 (2012) 3776-3788.

[8] L. Zhu, S. Ang, A.W.-T. Liu, Appl. Environ. Microbiol. 70 (2004) 597-598.

[9] A.D. Saran, M.M. Sadawana, R. Srivastava, J.R. Bellare, Colloids Surf. A 384 (2011) 393-400.

[10] D.J. Bharali, D.W. Lucey, H. Jayakumar, H.E. Pudavar, P.N. Prasad, J. Am. Chem. Soc. 127 (2005) 11364-11371.

[11] P.K. Santra, P.V. Kamat, J. Am. Chem. Soc. 134 (2012) 2508-2511.

[12] S.F. Wuister, I. Swart, F. van Driel, S.G. Hickey, C. de Mello Donegá, Nano Lett. 3 (2003) 503-507.

[13] L. Dworak, V.V. Matylitsky, V.V. Breus, M. Braun, T. Basché, J. Wachtveitl, J. Phys. Chem. C 115 (2011) 3949-3955.

[14] R. Zeng, M. Rutherford, R. Xie, B. Zou, X. Peng, Chem. Mater. 22 (2010) 2107-2113.

[15] C.S. Yang, Y.J. Lai, W.C. Chou, W.K. Chen, M.C. Lee, M.C. Kuo, J. Lee, J.L. Shen, D.J. Jang, Y.C. Cheng, J. Appl. Phys. 97 (2005) 033514.

[16] P. Reiss, M. Protière, L. Li, Small 5 (2009) 154-168.

[17] Z. Deng, H. Yan, Y. Liu, J. Am. Chem. Soc. 131 (2009) 17744-17745.

[18] R.E. Bailey, S. Nie, J. Am. Chem. Soc. 125 (2003) 7100-7106.

[19] J. Cheng, D. Li, T. Cheng, B. Ren, G. Wang, J. Li, J. Alloy Compd. 589 (2014) 539-544.

[20] N.H. Yen, W.D. de Marcillac, C. Lethiec, P.N. Hong, C. Schwob, A. Maître, N.Q. Liem, L.V. Vu, P. Bénalloul, L. Coolen, P.T. Nga, Opt. Mater. 36 (2014) 1534-1541.

[21] W.K. Bae, M.K. Nam, K. Char, S. Lee, Chem. Mater. 20 (2008) 5307-53.

[22] H. Shen, S. Wang, H. Wang, J. Niu, L. Qian, Y. Yang, A. Titov, J. Hyvonen, Y. Zheng, L.S. Li, Appl. Mater. Interfaces 5 (2013) 4260-4265.

[23] F. Yang, P. Pang, L. Zhang, Luminescence 28 (2013) 836-841.

[24] F. Yang, Z. Xu, J. Wang, F. Zan, C. Dong, J. Ren, Luminescence 28 (2013) 392-400.

[25] D. Magde, R. Wong, P.G. Seybold, Photochem. Photobiol. 75 (2002) 327-334.

[26] I. Mekis, D.V. Talapin, A. Kornowski, M. Haase, H. Weller, J. Phys. Chem. B 107 (2003) 7454-7462.

[27] J. Li, Y. Wang, W. Guo, J.C. Keay, T.D. Mishima, M.B. Johnson, X. Peng, J. Am. Chem. Soc. 125 (2003) 12567-12575.

[28] O. Chen, J. Zhao, V.P. Chauhan, J. Cui, C. Wong, D.K. Harris, H. Wei, H.-S. Han, D. Fukumura, R.K. Jain, M.G. Bawendi, Nat. Mater. 12 (2013) 445-451.

[29] C.-T. Cheng, C.-Y. Chen, C.-W. Lai, W.-H. Liu, S.-C. Pu, P.-T. Chou, Y.-H. Chou, H.-T. Chiu, J. Mater. Chem. 15 (2005) 3409-3414.

[30] M. Geszke-Moritz, M. Moritz, Mater. Sci. Eng. C-Mater. 33 (2013) 1008-1021.

[31] B.O. Dabbousi, J. Rodriguez-Viejo, F.V. Mikulec, J.R. Heine, H. Mattoussi, R. Ober, K.F. Jensen, M.G. Bawendi, J. Phys. Chem. B 101 (1997) 9463-9475.

[32] w. Zhang, G. Chen, J. Wang, B.-C. Ye, X. Zhong, Inorg. Chem. 48 (2009) 9723-9731.

[33] R. Xie, K. Chen, X. Chen, X. Peng, Nano Res. 1 (2008) 457-464.

[34] M. Jones, S.S. Lo, G.D. Scholes, Proc. Natl. Acad. Sci. U.S.A. 106 (2009) 3011–3016.

[35] N. Durisic, A.G. Godin, D. Walters, P. Grütter, P.W. Wiseman, C.D. Heyes, ACS Nano 5 (2011) 9062-9073.